TECHNISCHE MECHANIK
an open access journal

journal homepage: www.ovgu.de/techmech

Tech. Mech., Vol. 43, Is. 1, (2023), 73–82

Received: 14.02.2023
Accepted: 15.02.2023
Available online: 16.02.2023

Langevin Dynamics Prediction of the Effect of Shear Rate on Polymer-Induced Flocculation

L.F. Mortimer [1]*, M. Fairweather [1]

[1] School of Chemical and Process Engineering, University of Leeds, Woodhouse, Leeds LS2 9JT

Abstract: A novel potential-based model for resolving polymer-particle interaction in flows is presented and used to study the effect of shear rate on the adsorption dynamics of polymer chains onto a stationary spherical particle surface. The polymeric phase is modelled as a sequence of bead-spring components using Langevin dynamics with the finite extensible nonlinear elastic (FENE) potential to represent the molecular interactions within the polymer chain. The effects of steric interactions and the Kratky-Porod bending rigidity potential are also included in the calculations. Particles are modelled as rigid computational spheres which interact sterically with the polymer beads through a modified, truncated Lennard-Jones potential. Dependencies of conformation properties such as the mean radius of gyration and end-to-end distance on the diffusion coefficient, bending rigidity and the shear flow rate are discussed and their implications on the collision cross section for polymer-particle interactions are considered. Polymer-particle adsorption events are studied, and it is shown from Monte-Carlo studies that low shear encourages full adsorption at the point of collision, whereas increased shear hinders it, with moderate shear causing shorter tail-like structures upon adsorption. Increasing the bending rigidity potential strength leads to higher adsorption rates, with rigid polymers more likely to form tails. At both low and high FENE potential strengths, an increase in adsorption efficiency as well as the frequency of tail-like final conformities is observed. The findings of this study are of importance to the development of behavioural modification techniques where bulk system parameters are tuned to obtain a desired behaviour in important industrial processes such as flocculation and settling.

Keywords:

1 Introduction

The addition of small concentrations of high-molecular-weight polymers to particle-laden flows to separate non-settling fine solids from aqueous suspensions is a promising technique to instigate settling, suitable for many industrial challenges and requirements such as filtration and thickening (Lockwood et al., 2021; Vajihinejad et al., 2019; Lee et al., 2014). Despite demonstration in laboratory-scale rigs and wastewater flows, the dynamics leading to flocculation in such systems are still poorly understood (Dickinson and Eriksson, 1991). In such applications, natural flocculants are usually combined with synthetic polymers to tailor the additive properties to those required for maximum efficiency, with the process of doing so referred to as behavioural modification. However, without the ability to predict the system parameters which best exhibit a required outcome, these techniques are still performed inefficiently. Furthermore, the potential to use polymers in sensitive systems such as nuclear waste processing flows and water treatment depends upon on the development of improved understanding and demonstrable effectiveness. Particles in such flows are usually in the micro- or nano-range and therefore flocculation is used to increase the mean particle size for improved solids removal. In recent decades, the application of various polymeric-phase modelling techniques (Oettinger, 2012) has uncovered remarkable behaviours in simple interacting systems such as stagnant tanks (Smith et al., 1999), as well as in shear and turbulent flows (Fu and Kawaguchi, 2013). Polymer-particle interaction is also of use in the polymer synthesis industry, since nanoparticles have been shown to influence various properties of polymer nanocomposites such as viscosity (Mackay et al., 2003), glass transition temperature (Starr et al, 2001) and electrical conductivity (White et al., 2010).
Monte-Carlo modelling has shown that the resulting polymer-particle structure is highly dependent on the strength of the interaction potentials (Li et al., 2016), with the relative proportion of trains to tails and loops increasing with interaction strength. Similar studies also indicate that the polymer chain length is an important parameter when predicting the critical adsorption point (Li et al., 2012). Despite reasonable progress in recent studies, many questions remain unanswered surrounding the dynamics leading to polymer-particle bridging and subsequent flocculation, particularly so in non-stagnant systems, where shear has been shown to play an important role in polymer conformation (He et al., 2010). Polymers within shear flows have been shown experimentally to undergo both elongational and rotational mechanisms which lead to tumbling motions, increasing the complexity of polymer-particle interaction behaviour (He et al., 2009). The final flocculant structure has been shown to be sensitive to polymer properties, with porous flocculated structures capable of being broken by fluid shear (Tambo, 1991). This study aims to use nonequilibrium Langevin dynamic simulations to elucidate the fundamentals of polymer-particle interaction and adhesion within shear flows, as well as the way in which chemical or bulk properties (such as ionic strength which modulates the molecular interaction potentials and shear rate which affects the conformity of the polymer chain) affect the dynamics of adhesion, bridging and subsequent flocculation. The development of the present technique also provides a foundation to study more complex rheological flows through interaction with the fluid stress tensor based on local polymer conformation. This allows for further

* E-mail address: l.f.mortimer@leeds.ac.uk
doi: 10.24352/UB.OVGU-2023-046

study of processes such as drag reduction and viscoelasticity.

2 Methodology

In the present work, Langevin dynamics is used to simulate polymers as macromolecular chains of interacting beads (monomers), as employed in various Brownian dynamic studies (Doyle et al., 1998; Brackley, 2020; Li et al, 2017). The position vector $\boldsymbol{r}_i$ of each bead (referenced using subscript i) in a polymer chain evolves by obeying the following Newtonian equation of motion (Oettinger, 2012):

$$m_b \frac{d^2 \boldsymbol{r}_i}{dt^2} = -\boldsymbol{\nabla} V_i - \xi \left(\frac{d\boldsymbol{r}_i}{dt} - \boldsymbol{u}_{F,i} \right) + \sqrt{2 k_B T \xi}\, \boldsymbol{\eta}_i(t). \tag{2.1}$$

Here, m_b represents the mass of the bead, t is time, V_i is the total interaction potential calculated at the bead's current position, ξ is the drag coefficient, $\boldsymbol{u}_{F,i}$ is the local fluid velocity, k_B is the Boltzmann constant, T is the temperature and $\boldsymbol{\eta}_i(t)$ is a Brownian noise term satisfying $\langle \eta_{ia}(t) \rangle = 0$ and $\langle \eta_{ia}(t)\, \eta_{ib}(t') \rangle = \delta_{a,b}\, \delta(t - t')$. If a constant bead diameter is used, σ_b, then time may be nondimensionalised using the Brownian bead timescale $\tau_b = \sqrt{m_b \sigma_b / k_b T}$, and space using the bead diameter. Further introducing the diffusion coefficient, $D = k_B T / \xi$, allows us to rewrite Eq. (2.1) as:

$$\frac{d^2 \boldsymbol{r}_i^*}{dt^{*2}} = -\boldsymbol{\nabla} V_i^* - \xi \left(\frac{d\boldsymbol{r}_i^*}{dt^*} - \boldsymbol{u}_{F,i}^* \right) + \sqrt{\frac{2}{D}}\, \boldsymbol{\eta}_i^*(t^*), \tag{2.2}$$

where variables superscripted with (*) represent nondimensional terms. The contributions to the overall interaction potential for the beads are given by:

$$V_i^* = V_{i,F}^* + V_{i,B}^* + V_{i,W}^* + V_{i,P}^*. \tag{2.3}$$

The first term $V_{i,F}^*$ represents the bonds between the monomers using the finitely extensible nonlinear elastic (FENE) spring force described using the potential:

$$V_{i,F}^*(\delta r^*) = -\frac{K_F^* R_0^{*2}}{2} \ln \left[1 - \left(\frac{\delta r^*}{R_0^*} \right)^2 \right], \tag{2.4}$$

where $\delta r^* = |\boldsymbol{r}_{i+1}^* - \boldsymbol{r}_i^*|$ is the bead separation, K_F^* is the FENE energy scale and R_0^* is the maximum FENE bond length. This interaction potential is only included in the calculation of neighbouring beads in the chain of monomers. The second term is used to model the effects of polymer bending rigidity observed in real polymers, wherein acute polymer angles are less favoured energetically due to molecular constraints. The Kratky-Porod potential is given by:

$$V_{i,B}^*(\theta_i) = K_B^* \left(1 + \cos \theta_i \right), \tag{2.5}$$

where θ_i is the angle formed by two neighbouring separation vectors, i.e. $\theta_i = \cos^{-1}(\hat{\boldsymbol{n}}_{i+1} \cdot \hat{\boldsymbol{n}}_i)$ with $\hat{\boldsymbol{r}} = (\boldsymbol{r}_i^* - \boldsymbol{r}_{i+1}^*)/|\boldsymbol{r}_i^* - \boldsymbol{r}_{i+1}^*|$. K_B represents the strength of the bending rigidity. The penultimate term in Eq. (2.3) represents steric interactions between polymer beads and is given by a Weeks-Chandler-Anderson (WCA) potential:

$$V_{i,W}^*(\delta r^*) = 1 + 4 \left[\left(\frac{1}{\delta r^*} \right)^{12} - \left(\frac{1}{\delta r^*} \right)^6 \right], \tag{2.6}$$

which contributes to the total potential for all pairs of monomers within a maximum distance δr_{max}^*. The final term represents interaction with a dispersed particulate phase. Particles are represented by rigid body isotropic spheres of constant diameter, $D_P = 5\,\sigma_b$. In all simulations considered here the particle remains fixed at the midpoint of the computational domain. Polymer beads close to the particle are able to interact sterically. The polymer-particle interaction potential is a truncated Lennard-Jones (LJ) potential which takes the form (Li et al, 2017):

$$V_{i,P}^*(\delta r^*) = K_{LJT}^* \left[\left(\frac{1}{\delta r^* - s^*} \right)^{12} - 2 \left(\frac{1}{\delta r^* - s^*} \right)^6 \right] + V_{0,P}^*, \tag{2.7}$$

with the term $V_{0,P}^*$ representing a shift in the interaction potential such that $V_{i,P}^*(\delta r^* > 5) = 0$, given as:

$$V_{0,P}^*(\delta r^*) = K_{LJT}^* \left[\left(\frac{1}{2.5} \right)^{12} - 2 \left(\frac{1}{2.5} \right)^6 \right]. \tag{2.8}$$

To solve Eqs. (2.2-2.8), the Verlet-velocity integration method was employed with constant timestep δt^*. For shear flows, the shear rate is parameterised by the Weissenberg number based on the bead timescale, $We = \tau_b\, du/dy = du^*/dy^*$. The domain in all cases is a $90 \times 30 \times 90$ computational channel cell, ensured to be much larger than the polymer radius of gyration, as well as the

particle. Periodic conditions are enforced in the streamwise (x^*) and spanwise (z^*) directions, and a wall potential at the extents of the y^* direction, with form:

$$V_W^*(\delta y^*) = 10\ \delta y^{*2}, \tag{2.9}$$

with δy^* the wall penetration distance. The domain for polymer-particle interaction is illustrated in Figure 2.1. In the case of shear flows, the lower wall ($y^* = 0$) possesses a constant streamwise velocity of $u_x^* = 0$ everywhere on the wall, and the top wall is kept at $u_x^* = 30\ We$, with the gradient constant within the domain. The particle diameter is fixed at $D_P^* = 10$.

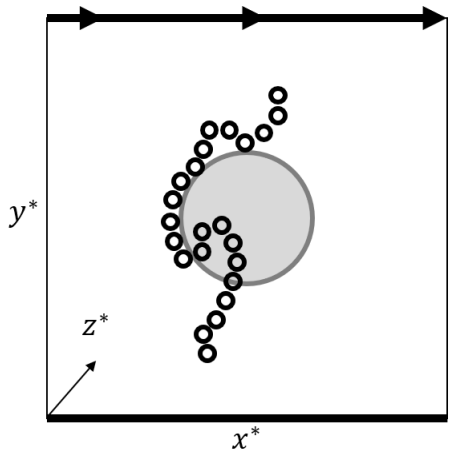

Fig. 2.1: Schematic of polymer-particle adsorption event within a cell. The particle is represented by the large grey circle, while polymer beads are represented by small white circles. Thick black arrowed lines represent direction and magnitude of shear flow.

3 Results and Discussion

We first consider the tuneable parameters in our model, of which there are many. The number of beads in a polymer chain is fixed at $N_B = 32$. To complement previous studies (Brackley, 2020), both the FENE potential and the maximum FENE bond length are fixed, with $K_F^* = 30$ and $R_0^* = 1.6$, though variation of the FENE potential will be discussed later. The impact of these parameters on the components of the individual bead-bead interaction potentials as well as their total as a function of separation distance is illustrated in Figure. 3.1. Here, a stable minimum is observed at just below $\delta r^* = 1.0$, which would be the equilibrium separation without the influence of Brownian forces or fluid interaction. The effect of the bending rigidity strength on the full potential as a function of chain angle is also illustrated in Figure 3.2. For increased strengths, the minima at more obtuse angles becomes more stable, hence less bending between the polymer beads is expected leading to more straightened-out conformities. Polymer rigidity has been shown to play an important role in adsorption conformity in molecular dynamics simulations (Kramarenko et al., 1996) such that stiffer chains adsorb more easily onto planar surfaces, hence the effect of this parameter will also be studied.

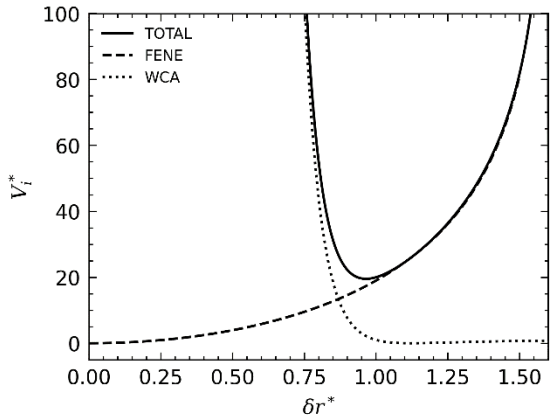

Fig. 3.1: Interaction potentials for neighbouring polymer beads with $K_F^* = 30$ and $R_0^* = 1.6$.

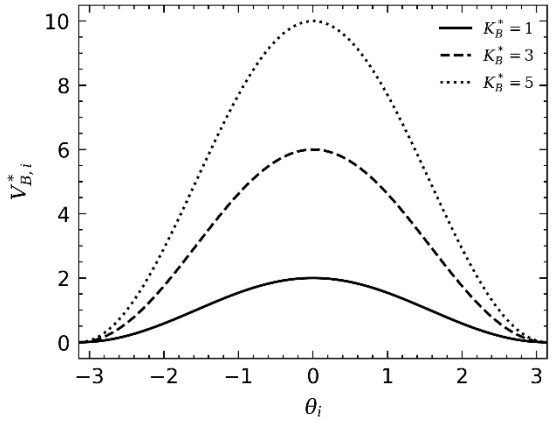

Fig. 3.2: Effect of bending rigidity, K_B^*, on interaction potential for neighbouring polymer beads.

Initial simulations were performed under quiescent conditions in order to determine how the bending rigidity, K_B^*, affects the conformity of the polymer. The effect of variation of the diffusion coefficient, D, was also considered, which determines the extent of friction damping within the system. For all simulations presented here, Monte-Carlo techniques were employed, meaning that multiple instances of the same simulation were performed with measurables averaged over all instances. For the quiescent simulations, 1000 samples were obtained with individual polymers injected into a stagnant cell and allowed to disperse freely. The timestep remained constant at $\delta t^* = 0.005$.

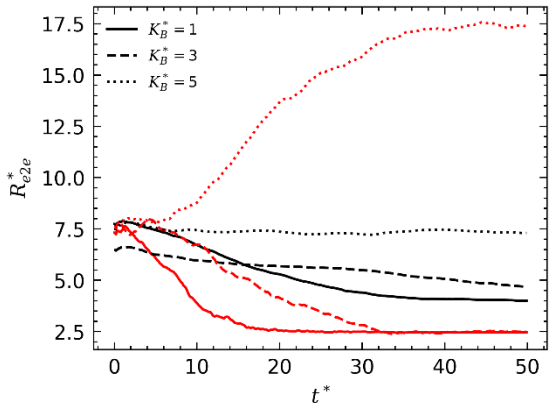

Fig. 3.3: Effect of bending rigidity, K_B^*, and diffusion coefficient, D, on temporal evolution of end-to-end polymer chain distance under quiescent conditions. Black: $D = 0.5$, Red: $D = 5$.

The effect of K_B^* and D on the temporal evolution of the mean end-to-end polymer chain distance is illustrated in Figure 3.3. The system exhibits the greatest elongational behaviour when both the bending rigidity and the diffusion coefficient are greatest, with the increase in D having the greatest effect when compared to the overdamped $D = 0.5$ system. In the other two cases, at $K_B^* = 3$ and $K_B^* = 1$, the variation of diffusion coefficient had the opposite effect, meaning that the larger coefficient systems exhibited lower polymer end-to-end separations. This is likely due to the dominance of the Brownian term in Eq. (2.2) leading to more compact conformity states where bending rigidity plays a less important role. This is clear for the low damping system with $K_B^* = 3$ and $K_B^* = 1$ where the eventual mean end-to-end distance vectors are very similar. The mean radius of gyration associated with a polymer chain was calculated using:

$$R_{0,i}^* = \sqrt{\frac{1}{N_B} \sum_i \left(\boldsymbol{r}_i^* - \overline{\boldsymbol{r}}^*\right)^2}, \tag{3.1}$$

with $\boldsymbol{r}_i^*$ the position of bead i and $\overline{\boldsymbol{r}}^*$ the mean bead position. The temporal evolution of the mean of this quantity is illustrated in Figure 3.4. Once again, the system with the high diffusion coefficient and bending rigidity exhibited large radii of gyration and the greatest deviation between the damped and undamped cases.

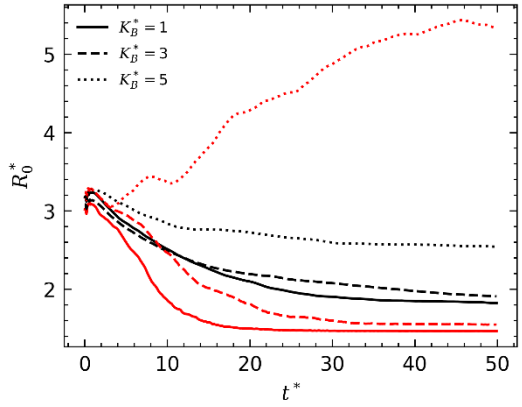

Fig. 3.4: Effect of bending rigidity, K_B^*, and diffusion coefficient, D, on temporal evolution of polymer chain radius of gyration under quiescent conditions. Black: $D = 0.5$, Red: $D = 5$.

From Figures 3.4 and 3.3 it is clear that polymers in these cases are stretching and forming long elongated strands. For lower bending rigidities, varying the diffusion coefficient has a much more pronounced effect than varying the rigidity, with the most curled-up polymers occurring in the undamped, low rigidity case. Here beads are able to visit locations close to the polymer centre of volume during their random diffusion, with little tendency to extend away from their neighbouring beads.

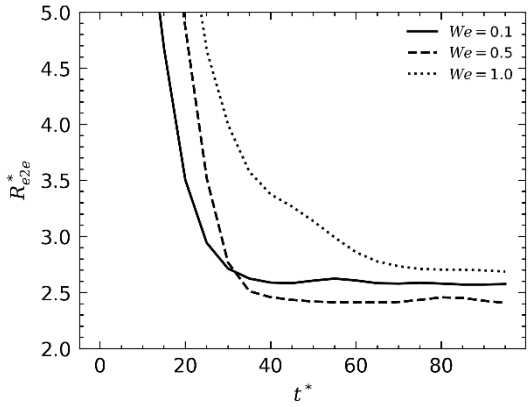

Fig. 3.5: Effect of Weissenberg number, We, on temporal evolution of end-to-end polymer chain distance under shear flow conditions.

To investigate the effect of Weissenberg number, We, on the conformation properties of polymers, subsequent simulations were performed in a shear flow within the domain outlined in Figure 2.1. This time, the diffusion coefficient was set as constant with $D = 5$ (i.e. the most curled polymers and largest variation in stretching behaviour under quiescent conditions) in order to isolate stretching effects due to polymer properties and system conditions such as shear rate. Root beads were initially injected into a random location within the domain and allowed to 'grow' randomly ensuring that the following bead was located on a surrounding unit sphere. Grown beads were also not permitted to overlap. The temporal evolution of the mean end-to-end distance as a function of We is illustrated in Figure 3.5. This property is maximised for the highest shear rate, meaning the velocity gradient across the polymer chain induces stretching. Interestingly, for the midrange shear, R_{e2e}^* is actually reduced. Tumbling behaviour was observed, consistent with previous studies (Chopra and Larson, 2002), which counteracted the extensional behaviour associated with the shear, wherein chains would begin to extend and then, due to the torque applied by the variation in fluid velocity across the chain, would begin to rotate. When the chains are orientated streamwise there is no longer any velocity gradient across the polymer and hence the curling mechanisms can occur, bringing the two ends of the polymer closer together. At the lowest shear rate, this curling dynamic is dominant (as in the quiescent condition) but the polymer chain contracts in on itself across the full chain, offering greater distance between the start and end beads. In Figure 3.6, the effect on the radius of gyration of the resulting conformities is clear. For high Weissenberg number, the polymers adopt more elongated states, with intermediate distances between beads generally larger. Even though the mean end-to-end distance is lowest for $We = 0.5$, the radius of gyration remains moderate, which implies slightly elongated spherical conformities (which was confirmed by visual inspection of the systems). Finally, for low Weissenberg number, R_0^* remains low, as the chains form tightly bound conformities.

Fig. 3.6: Effect of Weissenberg number, We, on temporal evolution of polymer chain radius of gyration under shear flow conditions.

If an applied shear flow causes the polymer radius of gyration to increase, it is expected that the collision cross section between polymers and particles would increase for flocculation applications. However, it is also known from the literature that there exists competition between coagulation and fragmentation, which depends highly on the shear rate (Spicer and Pratsinis, 1996). To

elucidate further the dynamics at the point of polymer-particle impact and interaction, the effect of Weissenberg number, bending rigidity and FENE potential strength on the adsorption of polymer chains onto a spherical particle was also studied. In these simulations, a single particle was fixed in the centre of the domain, with bead-particle interactions governed by the LJ force as in Eq. (2.7). Parameters for these simulations are presented in Table 3.1.

Parameter	Value
We	0.1, **0.5**, 1.0
R_0^*	1.6
D	5
K_F^*	10.0, **30.0**, 50.0
K_B^*	**1.0**, 3.0, 5.0
K_P^*	10.0
δt^*	0.005
N_B	32

Tab. 3.1: Polymer-particle adsorption simulation parameters. Parameters indicated in bold represent fixed 'base case' conditions when other parameters are varied.

In each Monte-Carlo instantiation, a single polymer was injected at a random location with a conformation chosen at random from the samples obtained in the polymer-only systems. This initial position means that the shear flow would direct the polymer towards the particle in time. This chosen setup aims to capture a single polymer-particle interaction event typical of those taking place in shear and turbulent flows. Once injected, the simulation is allowed to evolve for a set amount of time ($t^* = 15$). The final positions of each bead were then recorded, with some instances ending with polymer-particle adsorption and some without. Examples of three typical eventualities for each Weissenberg number are presented in Figure 3.7. The left plot demonstrates the low shear ($We = 0.1$) simulation, where most of the beads have clearly adsorbed onto the surface of the particle. Given the spherical 'ball' nature of the conformity of these polymers, collisions with the particle are likely and the lack of flow strength allows the chain to unravel across the particle. The middle plot illustrates a typical medium shear example, where some beads in the polymer chain have successfully adsorbed onto the particle, but the full polymer remains curled and has not fully unravelled. Finally, in many cases at high shear, $We = 1.0$, the polymers are unsuccessful in adsorbing onto the particle. In some cases temporary adsorption was observed, but the shear flow was strong enough to remove the polymer from the particle.

Fig. 3.7: Instantaneous snapshots of $t^* = 15$. Effect of We on eventual polymer adsorption state is indicated with $We = 0.1$ (left), $We = 0.5$ (middle) and $We = 1.0$ (right).

To further quantify the extent of polymer bead adsorption, an adsorption condition is defined such that the surface-to-surface distance between a polymer bead and the particle is lower than an arbitrary value $\sigma_A = 2$. Table 3.2 shows the percentage of instantiations resulting in at least one polymer bead remaining adsorbed onto the particle surface. For low shear, over half the interactions resulted in adsorption, whereas as the Weissenberg number increases, the occurrence of adsorption becomes increasingly unlikely. In the case of $We = 1.0$, the shear is too strong for beads to remain bound to the particle surface, and it is likely that any instances of adsorption at the sample time was due to their random walk being close to the particle.

We	% Adsorption
0.1	67
0.5	38
1.0	12

Tab. 3.2: Adsorption efficiency dependence on Weissenberg number.

To further examine the conformity of the chain at the particle surface, the probability density function for the number of adsorbed beads in each polymer chain, N_A, sampled over all 100 Monte-Carlo instances is presented in Figure 3.8. Starting with the low shear rate system, these interactions exhibited the most $N_A = N_B = 32$ (i.e. full adsorption) events where all beads in the chain remained bound to the surface. The distribution is also fairly uniform, and so there existed some interactions where only a few of the beads fully adsorbed and others where the chain failed to adsorb at all.

Fig. 3.8: Probability density function of the number of adsorbed beads N_A. Effect of Weissenberg number is illustrated.

As the shear rate increases, the number of fully adsorbed chains is reduced and the number of chains in the region where fewer than half of the beads adsorb increases. This is indicative of tail- and train-like adsorption behaviour, where the particle has a polymer

chain attached, with a free end or loop still subject to fluid dispersion. Finally, the high shear system peaks at $N_A = 0$ indicating the dominance of events with no adsorption, however, there did still exist a few events exhibiting tail- and train-like behaviour. Lastly, to further quantify the existence of tails within the adsorbed state, N_T is defined as the number of 'tail' beads within a polymer chain which are connected to a 'free' end as well as an adsorbed bead. Connected in this case refers to an eventual neighbour further down the chain in either direction. The distribution of the number of tail beads in the adsorbed states is presented in Figure. 3.9.

Fig. 3.9: Probability density function of the number of tail beads N_T. Effect of Weissenberg number is illustrated.

Evidently, tails formed generally had $N_T < 10$ and were more common in the high shear systems because in the $We = 0.1$ system most beads were adsorbed onto the particle. It is also interesting that a secondary wide peak forms around $N_T = 20$ which likely corresponds to polymers with two tails and an adsorption region. Similar analysis of train-like (sequences of adsorbed beads) and loop-like (sequences of unadsorbed beads but attached at either end) behaviour was performed which indicated trains forming with low shear.

The above analysis was repeated, this time increasing the bending rigidity potential strength, K_B^*. For these simulations, the Weissenberg number and FENE potential strength were kept constant at $We = 0.5$ and $K_F^* = 30$. Table 3.3 details the adsorption percentage for the range of parameter values studied, which demonstrates highest adsorption efficiency at $K_B^* = 3$, although for increased rigidity adsorption is also likely. These findings are in agreement with the molecular dynamics simulations of Kramarenko et al. (1996), which observed increased adsorption for more rigid polymer chains.

K_B^*	% Adsorption
1	38
3	60
5	55

Tab. 3.3: Adsorption efficiency dependence on bending rigidity potential strength, K_B^*.

Considering probability density functions for the number of adsorbed monomers in Figure 3.10, it is observed that increasing the rigidity to $K_B^* = 3$ has the greatest effect in encouraging events where the entire polymer is absorbed upon the particle surface. Further increasing this parameter leads to an increase in events where only some of the polymer chain is adsorbed, an effect which could be desirable for subsequent multi-particle interactions and therefore flocculation purposes. This is further observed in Figure 3.11, where the distribution of the number of tail beads is skewed toward the higher end for increased bending rigidity. Since more rigid polymers are likely to sample states where intermonomer links are orientated in similar directions, it is likely that the cause of this is due to the energetically favourable conformity upon first adsorption whereby the rest of the chain orientates away from the particle. This explanation is best demonstrated in Figure 3.12, which illustrates a semi-adsorption event where the tail is unable to wrap around the particle, leading to a final condition where some of the polymer hangs away from the particle.

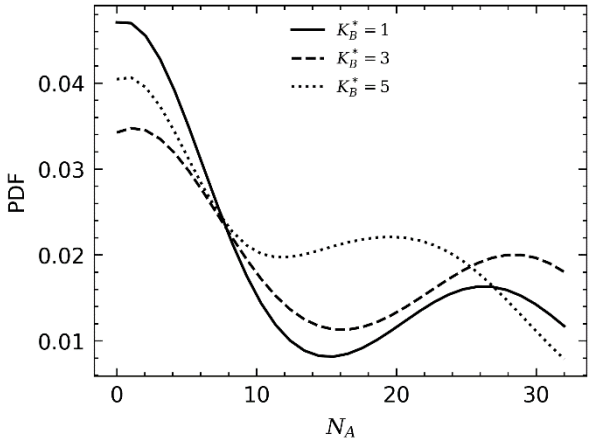

Fig. 3.10: Probability density function of the number of tail beads N_A. Effect of bending rigidity is illustrated.

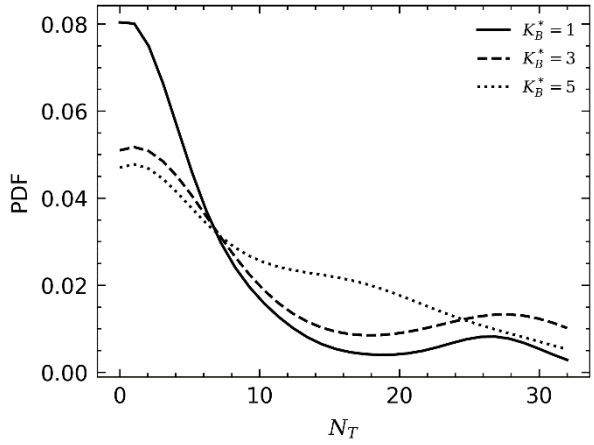

Fig. 3.11: Probability density function of the number of tail beads N_T. Effect of bending rigidity is illustrated.

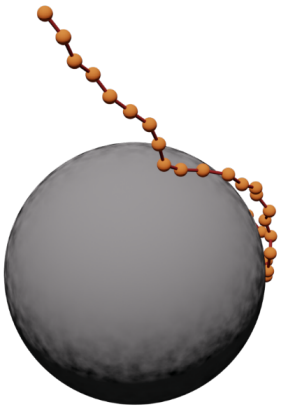

Fig. 3.12: Instantaneous final conformity example for $K_B^* = 3$, $We = 0.5$ and $K_F^* = 30$. Chain rigidity demonstrates difficulty in full adsorption since curling up on the particle is less energetically favourable.

The FENE potential strength is also an important parameter, since it represents the magnitude of the individual monomer-monomer link attraction, and affects the equilibrium state, meaning that for increased K_F^*, the monomers tend to remain closer to one another. Table 3.4 shows the adsorption efficiency for each parameter value studied.

K_F^*	% Adsorption
10	68
30	38
50	54

Tab. 3.4: Adsorption efficiency dependence on FENE potential strength.

In both cases, reducing or increasing the FENE potential strength leads to an increase in adsorption percentage. The distributions of the number of adsorbed beads, N_A, due to variation of the FENE potential strength is demonstrated in Figure 3.13. Though the distributions are similar, it is shown that for increased K_F^*, full adsorption is slightly more favourable, likely due to the beads tending to remain closer to each other, so upon initial adsorption, the following bead is more likely influenced to a state on the particle surface close to the initial bead. On the other hand, reducing K_F^* leads to a semi-adsorbed state being more likely. Since monomers are more likely to sample extended conformities, subsequent beads following initial adsorption may reside in locations where the LJ attraction is weaker, leading to tail-like final states. This is also observed in Figure 3.14, where tail-like conformities are more likely. Interestingly, the number of tail beads are also increased for $K_F^* = 50$, which is likely due to the effective increased rigidity since monomers are unable to overlap, hence the arguments for tails in more rigid chains previously discussed still apply.

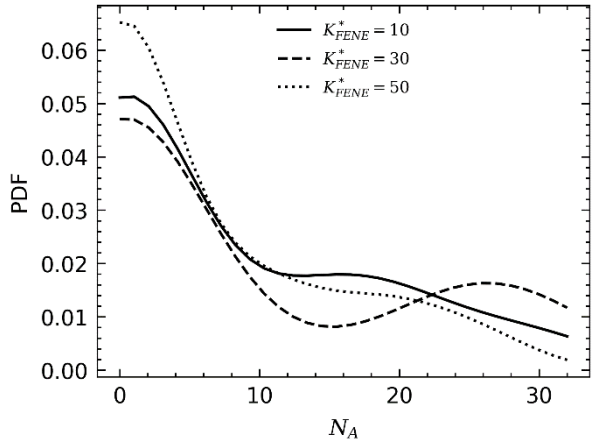

Fig. 3.13: Probability density function of the number of adsorbed beads N_A. Effect of FENE potential strength is illustrated.

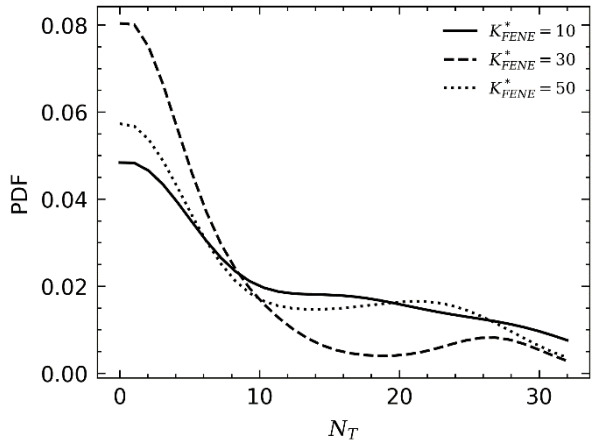

Fig. 3.14: Probability density function of the number of tail beads N_T. Effect of FENE potential strength is illustrated.

4 Conclusions

A novel potential-based particle-polymer adsorption simulation technique has been developed in order to explore the fundamentals of flocculation and polymer-surface interaction. The polymeric phase has been modelled using the FENE bead-spring approach and time-evolved using Langevin dynamics. Interactions within the polymer chain as well as the Kratky-Porod bending rigidity potential have been included in the calculations. The particle phase was modelled as a finite-size computational sphere, which interacts sterically with the polymer beads through a modified truncated Lennard-Jones potential.

From Monte-Carlo studies of quiescent conditions it was shown that polymers exhibit the greatest extensional behaviour when both the diffusion coefficient and the chain rigidity is high. For undamped systems, the influence of rigidity is very low below $K^*_B = 3$, whereas for damped systems, this parameter affects the eventual radius of gyration and mean end-to-end distance vector, with increased rigidity leading to more elongated conformities. Studies of polymers in shear showed that for high shear rates, chains were longer and possessed a larger radius of gyration. For medium shear, the polymers would undergo tumbling motion and the end-to-end distance vector would be reduced while their radius of gyration remained moderate. Finally, for the low shear system, conformities were generally ball-like and both properties were low.

Monte-Carlo simulations of shear flows in the presence of a single stationary particle were also performed to determine mechanisms for adsorption. Most adsorption took place in the low shear rate system, with beads able to resist the flow and unravelling across the particle surface. For the medium shear rate, some beads were able to adsorb onto the particle, forming tails and trains which increase the effective flocculation radius of the particle. For high shear rate, most beads were unable to adsorb onto the particle, with those successful often being removed later in the simulation. This is an interesting phenomenon for understanding the conditions which lead to most effective flocculation and should be studied further. Increasing the bending rigidity led to higher adsorption rates, with rigid polymers more likely to form tails, while both lowering and increasing the FENE potential strength caused an increase in adsorption efficiency as well as the occurrence of more tail-like final conformities. Another important parameter to consider in further studies is the polymer-particle LJ interaction strength, which can be influenced by modifying the ionic strength of the solution. In doing so, the effects of shear which reduce adsorption could be counterbalanced by stronger attraction between the polymer and the particles.

Using the techniques described in this paper, multi-particle simulations may also be performed to observe the way in which, and under what conditions, two or more particles begin to flocculate. Finally, the polymer contribution to the fluid stress tensor may also be included for study of more complex rheological measurements such as drag reduction, viscoelasticity and turbulence modulation (White and Mungal, 2008; Smith et al., 2002).

Acknowledgements

The authors are grateful for funding from the UK Engineering and Physical Sciences Research Council through the TRANSCEND (Transformative Science and Engineering for Nuclear Decommissioning) project (EP/S01019X/1).

References

Brackley, C. A., 2020. Polymer Compaction and Bridging-Induced Clustering of Protein-Inspired Patchy Particles, J Phys Condens Matter, Vol. 32, 314002.

Chopra, M., and Larson, R. G., 2002, Brownian Dynamics Simulations of Isolated Polymer Molecules in Shear Flow Near Adsorbing and Nonadsorbing Surfaces, J Rheol, Vol. 46, pp. 831-862.

Dickinson, E., and Eriksson, L., 1991, Particle Flocculation by Adsorbing Polymers, Adv Colloid Interface Sci, Vol. 34, pp. 1-29.

Doyle, P. S., Shaqfeh, E. S., and Gast, A. P., 1998, Rheology of Polymer Brushes: A Brownian Dynamics Study, Macromolecules, Vol. 31, pp. 5474-5486.

Fu, Z., and Kawaguchi, Y., 2013, A Short Review on Drag-Reduced Turbulent Flow of Inhomogeneous Polymer Solutions, Adv Mech Eng, Vol. 5, 432949.

He, G. L., Messina, R., and LÃ¶wen, H., 2010, Statistics of Polymer Adsorption Under Shear Flow, J Chem Phys, Vol. 132, 124903.

He, G. L., Messina, R., LÃ¶wen, H., Kiriy, A., Bocharova, V., and Stamm, M., 2009, Shear-Induced Stretching of Adsorbed Polymer Chains, Soft Matter, Vol. 5, pp. 3014-3017.

Kramarenko, E. Y., Winkler, R. G., Khalatur, P. G., Khokhlov, A. R., and Reineker, P., 1996. Molecular dynamics simulation study of adsorption of polymer chains with variable degree of rigidity. I. Static properties, J Chem Phys, Vol. 104, pp. 4806-4813.

Lee, C. S., Robinson, J., and Chong, M. F., 2014, A Review on Application of Flocculants in Wastewater Treatment, Process Saf Environ Prot, Vol. 92, pp. 489-508.

Li, C. Y., Cao, W. P., Luo, M. B., and Li, H., 2016, Adsorption of Polymer on an Attractive Nano-Sized Particle, Colloid Polym Sci, Vol. 294, pp. 1001-1009.

Li, H., Qian, C. J., and Luo, M. B., 2012, Simulation of a Flexible Polymer Tethered to a Flat Adsorbing Surface, J Appl Polym Sci, Vol. 124, pp. 282-287.

Li, C. Y., Luo, M. B., Li, H., and Cao, W. P., 2017, Simulation Study on the Conformational Properties of an Adsorbed Polymer on a Nanoparticle, Colloid Polym Sci, Vol. 295, pp. 2251-2260.

Lockwood, A. P. G., Peakall, J., Warren, N. J., Randall, G., Barnes, M., Harbottle, D., and Hunter, T. N., 2021, Structure and Sedimentation Characterisation of Sheared Mg (OH)2 Suspensions Flocculated with Anionic Polymers, Chem Eng Sci, Vol. 231, 116274.

Mackay, M. E., Dao, T. T., Tuteja, A., Ho, D. L., Van Horn, B., Kim, H. C., and Hawker, C. J., 2003, Nanoscale effects leading to non-Einstein-like decrease in viscosity. Nat Mater, Vol. 2, pp. 762-766.

Smith, D. E., Babcock, H. P., and Chu, S., 1999, Single-Polymer Dynamics in Steady Shear Flow, Science, Vol. 283, pp. 1724-1727.

Smith, G. D., Bedrov, D., Li, L., and Byutner, O., 2002. A molecular dynamics simulation study of the viscoelastic properties of polymer nanocomposites. J Chem Phys, Vol. 117, pp. 9478-9489.

Starr, F. W., Schroder, T. B., and Glotzer, S. C., 2001. Effects of a nano-sized filler on the structure and dynamics of a simulated polymer melt and the relationship to ultra-thin films. Phys Rev E, Vol 64, pp. 021802-021806.

Spicer, P. T., and Pratsinis, S. E., 1996, Shear-Induced Flocculation: The Evolution of Floc Structure and the Shape of the Size Distribution at Steady State, Water Res, Vol. 30, pp. 1049-1056.

Tambo, N., 1991, Basic concepts and innovative turn of coagulation/flocculation, Wat. Supply, Vol. 9, pp.1-10.

Oettinger, H. C., 2012, Stochastic Processes in Polymeric Fluids: Tools and Examples for Developing Simulation Algorithms, Springer-Verlag.

Vajihinejad, V., Gumfekar, S. P., Bazoubandi, B., Najafabadi, Z. R., and Soares, J. B. P., 2019, Water Soluble Polymer Flocculants: Synthesis, Characterization, and Performance Assessment, Macromol Mater Eng, Vol. 304, 1800526.

White, C. M. and Mungal, M. G., 2008. Mechanics and prediction of turbulent drag reduction with polymer additives. Annu. Rev. Fluid Mech, Vol 40, pp. 235-256.

White ,S. I., Mutiso, R. M., Vora, P. M., Jahnke, D., Hsu, S., Kikkawa, J. M., Li, J., Fischer, J. E., and Winey, K. I., 2010. Electrical percolation behavior in silver nanowire-polystyrene composites: simulation and experiment. Adv Funct Mater, Vol. 20, pp. 2709-2716.